

The solar zenith angle dependence of desert albedo

Zhuo Wang, Michael Barlage, and Xubin Zeng

Institute of Atmospheric Physics, University of Arizona, Tucson, Arizona, USA

Robert E. Dickinson

School of Earth and Atmospheric Sciences, Georgia Institute of Technology, Atlanta, Georgia, USA

Crystal B. Schaaf

Department of Geography, Boston University, Boston, Massachusetts, USA

Received 25 October 2004; revised 7 January 2005; accepted 8 February 2005; published 8 March 2005.

[1] Most land models assume that the bare soil albedo is a function of soil color and moisture but independent of solar zenith angle (SZA). However, analyses of the Moderate Resolution Imaging Spectroradiometer (MODIS) Bidirectional Reflectance Distribution Function (BRDF) and albedo data over thirty desert locations indicate that bare soil albedo does vary with SZA. This is further confirmed using the in situ data. In particular, bare soil albedo normalized by its value at 60° SZA can be adequately represented by a one-parameter formulation $(1 + C)/(1 + 2C * \cos(\text{SZA}))$ or a two-parameter formulation $(1 + B_1 * f_1(\text{SZA}) + B_2 * f_2(\text{SZA}))$. Using the MODIS and in situ data, the empirical parameters C , B_1 , and B_2 are taken as 0.15, 0.346 and 0.063. The SZA dependence of soil albedo is also found to significantly affect the modeling of land surface energy balance over a desert site. **Citation:** Wang, Z., M. Barlage, X. Zeng, R. E. Dickinson, and C. B. Schaaf (2005), The solar zenith angle dependence of desert albedo, *Geophys. Res. Lett.*, 32, L05403, doi:10.1029/2004GL021835.

1. Introduction

[2] Land surface albedo is an important factor in climate modeling, because it regulates the shortwave radiation absorbed by the surface. Surface albedo depends on soil characteristics and vegetation types. Error in the specification of soil albedo may cause biases in the computation of ground temperature and surface fluxes. In most land surface models (LSMs), the bare soil albedo is assumed to be a function of soil color and soil moisture but independent of solar zenith angle (SZA). Furthermore, most LSMs assume a uniform albedo over most desert areas.

[3] Satellite data have convincingly shown the significant geographic variation of desert albedo [Tsvetinskaya *et al.*, 2002; Wang *et al.*, 2004], and they can be directly used in LSMs to address the uniformity assumption above. Remote sensing data from the satellite and aircraft platforms as well as field measurements have also shown the anisotropy of bare soil surfaces, because soils have relatively opaque vertical structures that cause dark shadows [Kimes, 1983]. For instance, Monteith and Szeice [1961] showed that the measured bare soil albedo increases from 0.16 at 30° SZA to 0.19 at 70° SZA with a daily mean of 0.17. Idso *et al.*

[1975] found that, on average, the curves of albedo as a function of the SZA for wet and dry conditions are identical in shape. Ranson *et al.* [1991] compared the albedo computed from two integration methods with simultaneously acquired in situ data. The albedo obtained for the bare soil also increases for sun angles away from solar noon. The purpose of this study is to develop two simple formulations to represent the SZA dependence of bare soil albedo for weather and climate models and for the remote sensing retrieval of surface solar fluxes.

2. Data Analysis

[4] The global 0.05° Moderate-Resolution Imaging Spectroradiometer (MODIS) bidirectional reflectance distribution function (BRDF) and albedo Climate Modeling Grid (CMG) data (Version 4) are used in this study. The underlying 1-km BRDF/albedo data were derived by coupling all available cloud-free, atmospherically corrected, spectral surface reflectance observations over a 16-day period with a semi-empirical, kernel-driven BRDF model [Schaaf *et al.*, 2002]. The MODIS data are provided in three visible (460, 555, and 659 nm) and four near-infrared narrow bands (865, 1240, 1640, and 2130 nm), which are then used to infer the total shortwave (SW, $0.3\text{--}5.0\ \mu\text{m}$), visible (VIS, $0.3\text{--}0.7\ \mu\text{m}$), and near-infrared (NIR, $0.7\text{--}5.0\ \mu\text{m}$) broadband black-sky (or direct) and white-sky (or diffuse) albedos. These data are reprojected and averaged to a 0.05° grid, and the presence of snow and the quality of the majority of the BRDF inversions are stored for each gridbox. Only the data derived primarily from full inversion under snow-free condition are used. Furthermore, we analyze all of the BRDF data available from 2000 to 2004. Based on MODIS Land Cover Type (MOD12) and Fractional Vegetation Cover dataset derived from MODIS NDVI data, we have identified thirty 0.05° pixels over different desert areas with zero fractional vegetation cover to examine the SZA dependence of bare soil albedo. These pixels are selected to represent each of the major deserts of the world and their exact locations are available from the lead author.

[5] At each pixel, the black-sky albedo and its SZA dependence do not change much during all the 16-day periods. For instance, for the albedo at 60° SZA over a pixel (25.975°N , 5.075°E) in Africa, the interquartile ranges (IQRs); i.e., the differences between the 25th and 75th percentiles, are 0.013 and 0.010 for the VIS and NIR bands, respectively. Since the soil moisture effect on surface albedo

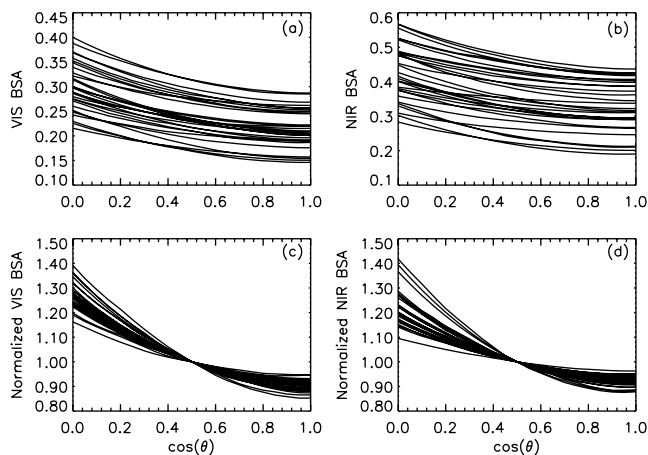


Figure 1. The median curves of the MODIS black-sky albedos in (a) VIS band and (b) NIR band versus the cosine of SZA at 30 desert locations. The normalized curves with respect to their albedo values at 60° SZA are shown in (c) VIS band and (d) NIR band.

would be minimal over this desert location, these small variations in black-sky albedo are probably primarily caused by the uncertainty of MODIS data themselves, although in some places, there may be a subpixel vegetation contribution as well. For each location, there is a median albedo among all the 16-day periods at each SZA, so a curve can be obtained from median albedos over all SZAs. Figures 1a and 1b show these median SZA dependence curves of black-sky albedo over all thirty pixels. The significant geographic variation of desert albedo is consistent with previous studies [Tsvetinskaya *et al.*, 2002; Wang *et al.*, 2004]. For instance, the IQRs of the black-sky albedos at 60° SZA are 0.065 and 0.116 in the VIS and NIR bands, respectively. To see the SZA dependence more clearly, we normalize each curve in Figures 1a and 1b by its value at 60° SZA, and results are shown in Figures 1c and 1d. While the albedo increases with SZA over each pixel, its variation with SZA is quantitatively different over different pixels.

[6] The SZA dependence of the MODIS surface albedo has been evaluated using field measurements which include a desert site at the Surface Radiation Budget Network. A case study over three stations reveals that the MODIS BRDF model is able to capture the SZA dependence of surface albedo as shown by the field measurements [Jin *et al.*, 2003]. Complementary to this study, here additional in situ data are used to further evaluate the MODIS data. We use the 0.05° (~ 5 km) MODIS data to compare with heritage field measurements collected at a single location. Figure 2a compares the MODIS data with surface measurements over a plowed field in Tunisia, Africa in April 1983 [Pinty *et al.*, 1989]. MODIS black-sky albedos are much higher than surface observations in both the VIS and NIR bands, possibly because of different surface conditions (including soil moisture) in April between 1983 and 2001 and because of the inherent difference between a point measurement and satellite measurements in a 0.05° grid. These differences are also contributed, to a lesser degree, by the comparison of the MODIS black-sky albedo with the in situ measurements of true albedo that is a weighted average of direct and diffuse albedos. To better compare the SZA

dependence, we normalize each curve in Figure 2a by its albedo at 60° SZA in Figure 2b. Evidently, both MODIS and in situ albedos increase with SZA and their SZA dependences are consistent with each other. Figures 2c and 2d compare MODIS data with the in situ data over an Avondale loam soil site in Phoenix, Arizona in May, July, September, and December 1973 [Idso *et al.*, 1975]. Over dry or wet soil, the observed in situ albedo minimum occurred near the smallest SZA at solar noon, while its maximum occurred at the greatest SZA in the morning and afternoon. The MODIS black-sky albedo and its SZA dependence in the SW band (i.e., the spectrally weighted average of VIS and NIR bands) agree with the in situ measurements over dry soil. Figures 2e and 2f compare the in situ albedo measurements of the tiger-bush soil over the Sahel desert in March and September 1990 [Allen *et al.*, 1994] with the MODIS SW albedo. It is unclear why the in situ albedo over wet soil actually decreases slightly with the increase of SZA for SZA greater than 60° . The in situ albedos over dry soil lie largely between the MODIS albedos in March and September 2001. However, the MODIS albedo increases faster with SZA than indicated by the in situ data.

3. Two Simple Formulations for the SZA Dependence of Bare Soil Albedo

[7] To adequately describe the SZA dependence of bare soil albedo as given in Figures 1 and 2, a new albedo

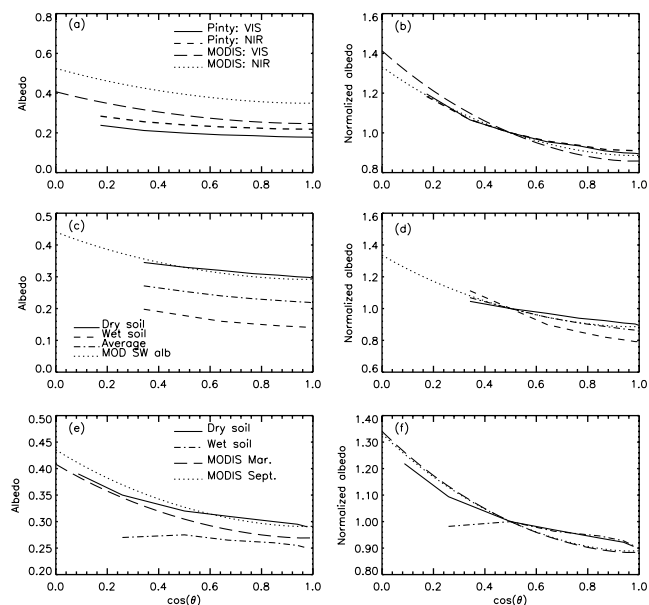


Figure 2. Comparison of MODIS data with in situ measurements. (a) The bare soil albedo in VIS and NIR bands versus cosine SZA in Tunisia, Africa in April 1983 [Pinty *et al.*, 1989]; (b) Same as (a) except for normalized black-sky albedos with respect to the albedo at 60° SZA; (c) The bare soil albedo in the SW band in Phoenix, Arizona in May, July, September, and December 1973 [Idso *et al.*, 1975]; (d) Same as (c) except for normalized black-sky albedos; (e) The bare soil albedo in the SW band over the Sahel desert in March and September 1990 [Allen *et al.*, 1994]; (f) Same as (e) except for normalized black-sky albedos.

formulation is derived here using the MODIS BRDF/albedo algorithm and data [Schaaf *et al.*, 2002]:

$$\alpha(\theta) = \alpha_r \cdot \{1 + B_1 \cdot [g_1(\theta) - g_1(60^\circ)] + B_2 \cdot [g_2(\theta) - g_2(60^\circ)]\} \quad (1)$$

where α is the black-sky albedo, θ is solar zenith angle, α_r is the albedo at 60° SZA and depends on season and location. The functions g_1 and g_2 are from the MODIS algorithm:

$$g_1(\theta) = -0.007574 - 0.070987\theta^2 + 0.307588\theta^3 \text{ and}$$

$$g_2(\theta) = -1.284909 - 0.166314\theta^2 + 0.04184\theta^3.$$

The parameters B_1 and B_2 are the average of the ratios of the volumetric and geometric parameters in the MODIS algorithm [Schaaf *et al.*, 2002] over α_r for 30 pixels, respectively. Figures 3a–3d shows these parameters in VIS and NIR bands for thirty pixels as a function of α_r . Based on this figure, we obtain $B_1 = 0.346$ and $B_2 = 0.063$.

[8] We have also tested the simple formulation [Briegleb *et al.*, 1986]:

$$\alpha(\theta) = \alpha_r \cdot \frac{1 + C}{1 + 2C \cdot \cos \theta} \quad (2)$$

where the empirical parameter C was taken as 0.4 for arable grass, grassland and desert, and 0.1 for all other types [Briegleb *et al.*, 1986]. Equation (2) and the above values for C have also been used in the remote sensing retrieval of land surface solar fluxes [Pinker and Laszlo, 1992] and in some land-atmosphere coupled models [e.g., Hou *et al.*, 2002].

[9] A more appropriate value for C can be determined by fitting each curve in Figures 1a and 1b to (2) by minimizing the integral over all SZA's for each 16-day period:

$$V = 2 \int_{\theta=0}^{\pi/2} \cos \theta \cdot \sin \theta \cdot (\alpha_M - \alpha_C)^2 d\theta \quad (3)$$

where α_M is the MODIS albedo and α_C is computed from (2). The weighting factor of $\cos \theta$ is the same as that used for computing the white-sky albedo [Schaaf *et al.*, 2002]. This is chosen also because MODIS data are more reliable at SZA less than 70° and because the albedo is more important at a smaller SZA when solar flux itself is large. The values for C over all thirty pixels are plotted as a function of α_r in Figures 3e and 3f. Their mean values for the VIS and NIR bands are 0.17 and 0.13, respectively, and their average of 0.15 is used for both bands to be consistent with Briegleb *et al.* [1986]. Furthermore, the best-fit linear equations can be obtained: $C_{\text{VIS}}(\alpha_r) = 0.29 - 0.51\alpha_r$ and $C_{\text{NIR}}(\alpha_r) = 0.13 - 0.02\alpha_r$. To compare the performance of (1) and (2), we compute $d = \left(\frac{1}{30} \sum_{i=1}^{30} V_i \right)^{1/2}$, where V_i is computed from (3)

for each of the 30 pixels. The values of d are 0.0061, 0.0081, and 0.0072 using the two-parameter model, one-parameter model with constant C as well as the best-fit linear equations, respectively. This shows that the two-parameter model is a little better than the one-parameter

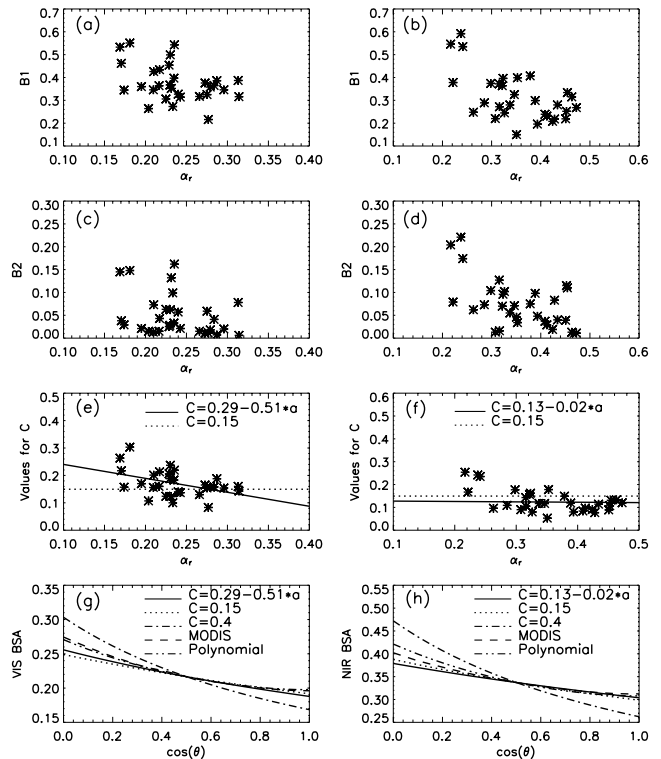


Figure 3. The median B_1 versus the MODIS black-sky albedos at 60° SZA (α_r) for 30 pixels in (a) VIS band and (b) NIR band. The median B_2 versus α_r in (c) VIS band and (d) NIR band. The values for C versus α_r in (e) VIS band and (f) NIR band (solid line: the best-fit linear function; dotted line: the average C value of VIS and NIR bands). (g) The SZA dependence at a pixel (19.975°N , 43.325°E) using the MODIS data directly and computed using (1) and (2) with different C (the best-fit linear function or fixed values) in the VIS band; (h) Same as (g) except in the NIR band.

model. If the white-sky albedo is used (i.e., without considering the SZA dependence), the d value would be 0.0195 and is much bigger than those using (1) or (2). This indicates the importance of the SZA dependence. Figures 3g and 3h evaluates the SZA dependence over a pixel (19.975°N , 43.325°E) using (1) and (2) with different values for C . The simulated SZA dependence using the two-parameter, one-parameter model with the best-fit linear equation or the C fixed at 0.15 are consistent with the MODIS data for SZA less than 60° . In contrast, the albedo computed with $C = 0.4$ increases with SZA much faster than indicated by the MODIS data, and its value at zero SZA is lower by 0.03 for the VIR band and 0.05 for the NIR band.

[10] We have further evaluated the impact of the prescribed parameters C , B_1 , and B_2 on the computed SZA dependence using the in situ data in Figure 2e. It is found that the deviations of the simulated albedo using (1) or (2) with $C = 0.15$ from in situ data are much smaller than those with $C = 0.4$ for SZA less than 70° (figure not shown). Based on these analyses, we recommend the use of the polynomial (1) or (2) with $C = 0.15$ over bare soil in land modeling and remote sensing retrieval of land surface solar fluxes. Then the white-sky albedo can be obtained analytically by integrating (1) and (2) over all SZA's [using

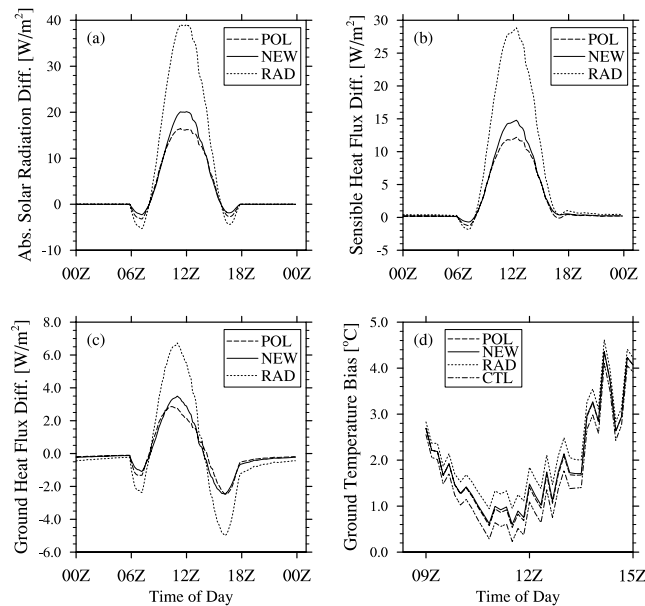


Figure 4. The sensitivity of the Noah land model to the SZA dependence of the bare soil albedo at a Sahel site. (a) Absorbed solar radiation difference between three different simulations and CTL; (b) Sensible heat flux difference; (c) Ground heat flux difference; and (d) Ground temperature bias of simulations from observations. See the text for the meaning of each simulation.

the weighting factor in (3)], and is $\alpha_{ws} = 0.97\alpha_r$ for (1) and $\alpha_{ws} = 0.96\alpha_r$ for (2).

4. Impact of the SZA Dependence of Soil Albedo on Land Modeling

[11] We have incorporated (1) and (2) into the Noah land surface model [Mitchell *et al.*, 2004]. The model is forced using observations over a tiger bush site from the Hydrologic Atmospheric Pilot Experiment in the Sahel [Goutorbe *et al.*, 1997]. We run the model from Aug. 20 to Sept. 30, 1992. The sensitivity of the Noah model to the SZA dependence of the albedo is shown in Figure 4. Four simulations are completed. The observed monthly averaged albedos for Aug., Sept., and Oct. are interpolated into the average daily albedo for these four runs. The control simulation (CTL) has no SZA dependence, similar to the offline Noah model setup. Equation (1) is used to define a SZA dependence ($B_1 = 0.346$, $B_2 = 0.063$) in the POL run. The NEW run uses (2) with $C = 0.15$. The RAD simulation is also done using (2) with $C = 0.4$, as implemented in the atmospheric radiative transfer scheme in the NCEP land-atmosphere coupled model [Hou *et al.*, 2002].

[12] Figure 4 shows the 5-day averaged diurnal cycle for the last 5 days of Sept. 1992. Compared with CTL, the SZA dependence formulations in (1) and (2) increase albedo at large SZA and decrease albedo at small SZA. Therefore, the absorbed solar radiation (Figure 4a) behaves as expected, with increases at solar noon of about 38, 20, and 16 W/m^2 for the RAD, NEW, and POL simulations, respectively. Since less solar radiation is incident at low sun angles, the SZA dependence does not affect the simulations much at sunrise and sunset. About 76% of the extra solar energy goes into an increase in sensible heat flux (Figure 4b) while another 18% is

transferred into the soil (Figure 4c). The remaining energy is primarily used to increase the ground temperature (Figure 4d) and is emitted as longwave radiation. Compared with CTL, the ground temperature at local solar noon is higher by 0.7°C, 0.4°C, and 0.3°C in the RAD, NEW, and POL simulations, respectively (Figure 4d). There are systematic temperature biases in all four simulations in comparison with observations (Figure 4d), but it goes beyond the scope of this study to further address this issue. Additional observational data from two sites in Arizona lead to similar conclusions.

[13] In summary, our analyses of the MODIS and in situ data indicate that bare soil albedo depends on the SZA, and this dependence can be adequately represented by (1) with $B_1 = 0.346$ and $B_2 = 0.063$ as well as (2) with $C = 0.15$. These dependences need to be considered in land modeling. Further work is also needed to evaluate the impact of these formulations on the remote sensing retrieval of land surface solar fluxes.

[14] **Acknowledgment.** This work was supported by NASA under grant NNG04GL25G and through its EOS IDS Program (429-81-22; 428-81-22), and by NOAA under grant NA03NES4400013.

References

- Allen, S. J., J. S. Wallace, J. H. C. Gash, and M. V. K. Sivakumar (1994), Measurements of albedo variation over natural vegetation in the Sahel, *Int. J. Remote Sens.*, **14**, 625–636.
- Briegleb, B. P., P. Minnis, V. Ramanathan, and E. Harrison (1986), Comparison of regional clear sky albedos inferred from satellite observations and model calculations, *J. Clim. Appl. Meteorol.*, **25**, 214–226.
- Goutorbe, J. P., et al. (1997), An overview of HAPEX-Sahel: A study in climate and desertification, *J. Hydrol.*, **188–189**, 4–17.
- Hou, Y. T., S. Moorthi, and K. Campana (2002), Parameterization of solar radiation transfer in the NCEP models, *NCEP Off. Note 441*, 34 pp., Natl. Cent. for Environ. Predict., Camp Springs, Md.
- Idso, S. B., R. D. Jackson, R. J. Reginato, B. A. Kimball, and F. S. Nakayama (1975), The dependence of bare soil albedo on soil water content, *J. Appl. Meteorol.*, **14**, 109–113.
- Jin, Y., C. B. Schaaf, C. E. Woodcock, F. Gao, X. Li, A. H. Strahler, W. Lucht, and S. Liang (2003), Consistency of MODIS surface bidirectional reflectance distribution function and albedo retrievals: 2. Validation, *J. Geophys. Res.*, **108**(D5), 4159, doi:10.1029/2002JD002804.
- Kimes, D. S. (1983), Dynamics of directional reflectance factor distributions for vegetation canopies, *Appl. Opt.*, **22**, 1364–1372.
- Mitchell, K. E., et al. (2004), The multi-institution North American Land Data Assimilation System (NLDAS): Utilizing multiple GCIP products and partners in a continental distributed hydrological modeling system, *J. Geophys. Res.*, **109**, D07S90, doi:10.1029/2003JD003823.
- Monteith, J. L., and G. Szeice (1961), The radiation balance of bare soil and vegetation, *Q. J. R. Meteorol. Soc.*, **87**, 159–170.
- Pinker, R. T., and I. Laszlo (1992), Modeling of surface solar irradiance for satellite applications on a global scale, *J. Appl. Meteorol.*, **31**, 194–211.
- Pinty, B., M. E. Verstrate, and R. E. Dickinson (1989), A physical model for predicting bidirectional reflectances over bare soil, *Remote Sens. Environ.*, **27**, 273–288.
- Ranson, K. J., J. R. Irons, and C. S. T. Daughtry (1991), Surface albedo from bidirectional reflectance, *Remote Sens. Environ.*, **35**, 201–211.
- Schaaf, C. B., et al. (2002), First operational BRDF, albedo nadir reflectance products from MODIS, *Remote Sens. Environ.*, **83**, 135–148.
- Tsvetinskaya, E. A., C. B. Schaaf, F. Gao, A. H. Strahler, R. E. Dickinson, X. Zeng, and W. Lucht (2002), Relating MODIS-derived surface albedo to soils and rock types over Northern Africa and the Arabian peninsula, *Geophys. Res. Lett.*, **29**(9), 1353, doi:10.1029/2001GL014096.
- Wang, Z., et al. (2004), Using MODIS BRDF and albedo data to evaluate global model land surface albedo, *J. Hydrometeorol.*, **5**, 3–14.

M. Barlage, Z. Wang, and X. Zeng, Institute of Atmospheric Physics, University of Arizona, Tucson, AZ 85721, USA. (zhuowang@atmo.arizona.edu)

R. E. Dickinson, School of Earth and Atmospheric Sciences, Georgia Institute of Technology, Atlanta, GA 30332–0340, USA.

C. B. Schaaf, Department of Geography, Boston University, Boston, MA 02215, USA.